A Journal of the Gesellschaft Deutscher Chemiker

Angewandte International Edition GDCh Chemie

www.angewandte.org

Accepted Article

Title: Grain Boundary Electronic Insulation for High-Performance All-Solid-State Lithium Batteries

Authors: Xiaofei Yang, Xuejie Gao, Ming Jiang, Jing Luo, Jitong Yan, Jiamin Fu, Hui Duan, Shangqian Zhao, Yongfu Tang, Rong Yang, Ruying Li, Jiantao Wang, Huan Huang, Xueliang Sun, and Chandra Veer Singh

To be cited as: *Angew. Chem. Int. Ed.* **2022**, e202215680

Link to VoR: https://doi.org/10.1002/anie.202215680

WILEY-VCH

10.1002/anie.202215680

WILEY-VCH

RESEARCH ARTICLE

Grain Boundary Electronic Insulation for High-Performance All-Solid-State Lithium Batteries

Xiaofei Yang‡[a], Xuejie Gao‡[a,b], Ming Jiang‡[c], Jing Luo[a], Jitong Yan[g], Jiamin Fu[a], Hui Duan[a], Shangqian Zhao[d], Yongfu Tang[g], Rong Yang[d], Ruying Li[a], Jiantao Wang*[d], Huan Huang*[e], Chandra Veer Singh*[f], Xueliang Sun*[a]

[a] Dr. X. Yang, Dr. X. Gao, Dr. J. Luo, J. Fu, Dr. H. Duan, R. Li, Prof. X. Sun
Department of Mechanical and Materials Engineering, University of Western Ontario, London, Ontario, N6A 5B9, Canada
E-mail: xsun@eng.uwo.ca (X. Sun)
[b] Dr. X. Gao
Liaoning Key Laboratory of Lignocellulose Chemistry and BioMaterials, College of Light Industry and Chemical Engineering, Dalian Polytechnic University, Dalian, 116034, China
[c] Dr. M. Jiang
Institute of Physical Science and Information Technology, Anhui University, Hefei 230601, China
[d] Dr. S. Zhao, Dr. R. Yang, Prof. J. Wang
China Automotive Battery Research Institute, Beijing, 100088, China
E-mail: wangjt@glabat.com (J. Wang)
[e] Dr. H. Huang
Glabat Solid-State Battery Inc.,700 Collip Circle, London, ON, N6G 4X8, Canada
E-mail: hhuang@glabat-ssb.com (H. Huang)
[f] Prof. C. V. Singh
Department of Materials Science and Engineering, University of Toronto, Toronto, Ontario, M5S 3E4, Canada
E-mail: chandraveer.singh@utoronto.ca (C. V. Singh)
[g] J. Yan, Prof. Y. Tang
Hebei Key Laboratory of Applied Chemistry, School of Environmental and Chemical Engineering, Yanshan University, Qinhuangdao 066004, China.
[‡] These authors contributed equally to this work.

Abstract: Sulfide electrolytes with high ionic conductivities are one of the most highly sought for all-solid-state lithium batteries (ASSLBs). However, the non-negligible electronic conductivities of sulfide electrolytes (~10^{-8} S cm^{-1}) lead to electron smooth transport through the sulfide electrolyte pellets, resulting in Li dendrite directly depositing at the grain boundaries (GBs) and serious discharge self-discharge. Here, a grain-boundary electronic insulation (GBEI) strategy is proposed to block electron transport across the GBs, enabling Li-Li symmetric cells with 30 times longer cycling life and Li-$LiCoO_2$ full cells with three times lower self-discharging rate than pristine sulfide electrolytes. The Li-$LiCoO_2$ ASSLBs deliver high capacity retention of 80% at 650 cycles and stable cycling performance for over 2600 cycles at 0.5 mA cm^{-2}. The innovation of the GBEI strategy provides a new direction to pursue high-performance ASSLBs depending on electronic conductivity regulation.

Introduction

All-solid-state lithium batteries (ASSLBs) using Li metal anode and high-ionic-conductivity solid-state electrolytes (SSEs) have attracted intensive research interest because of their improved safety and potential energy density beyond the state-of-the-art lithium-ion batteries (LIBs).[1] Among diverse SSE systems, sulfide SSEs have been regarded as one of the most promising candidates for ASSLBs application, because they present high ionic conductivity compared with solid polymer electrolytes (SPEs) and better electrode/electrolyte interfacial compatibility than rigid oxide SSEs.[2] Generally, the sulfide SSEs can be classified into two categories: high-valence-metal-element-containing sulfide SSEs (labeled as HVMECS-SSEs, e.g., $Li_{10}GeP_2S_{12}$ and $Li_{10}SnP_2S_{12}$) [3] and high-valence-metal-element-free sulfide SSEs (labeled as HVMEFS-SSEs, e.g., Li_6PS_5Cl, $Li_7P_3S_{11}$, and Li_3PS_4). [2b, 4] For the HVMECS-SSEs, the high-valence metal elements would react with Li anode rapidly and form a mixed electronic-ionic-conductive interface, resulting in the continuous decomposition of SSEs. [5] To suppress the side reactions, in most cases, a Li alloy or a buffer layer is introduced to separate the HVMECS-SSEs and Li anode for stable long-term cycling of ASSLBs. [6] Nevertheless, the use of Li alloys and buffer layers will decrease the energy density due to reduced working voltage and extra inert materials, respectively. For the HVMEFS-SSEs, side reactions also occur at the interface with the Li anode and produce an ionic-conductivity interface. Such an interface can serve as a solid-electrolyte interface (SEI) to ensure smooth Li^+ transport and suppress further side reactions between SSEs and Li anode. [7] Therefore, the HVMEFS-SSEs are a better choice to fulfill high-energy-density ASSLBs.

Despite the favorable properties of HVMEFS-SSEs in terms of high ionic conductivity and high compatibility with Li metal anodes, the concern of Li dendrite growth is hindering the pursuit of high-energy-density ASSLBs. [8] At the early research stage, some researchers attributed the cause to the mismatched Li/SSE interface that results in Li dendrite growth from the interface and then gradually penetrates through the bulk SSEs. Very recently, some noteworthy exceptions contradict the conventional “mismatched Li/SSE interface” concept.[8b, 9] Porz et al. observed Li dendrite growth even at the finely polished Li/SSE interfaces.[9] In another study, in-situ optical microscopy provided visual evidence that Li was directly deposited inside the Li_3PS_4 SSE.[8b] To clarify the underlying mechanism of Li dendrite in SSEs, Wang and his coworkers monitored the dynamic evolution of Li concentration profiles in three representative SSEs with different electronic conductivities by using time-resolved operando neutron depth profiling. Their results suggested that the non-negligible electronic conductivity of SSEs is the origin of Li dendrite growth in bulk SSEs.[10] This theory was adopted and further developed by Chi’s group.[11] They found that grain boundaries (GBs) have a reduced bandgap, where Li^+ is preferentially reduced by electrons to form local Li filaments, which could well explain the phenomenon of Li dendrite growth along the GBs. Based on this theory, blocking electron

10.1002/anie.202215680

transport at GBs can be regarded as an effective strategy to inhibit Li dendrites formation in ASSLBs. Moreover, the non-negligible electronic conductivity of SSEs and GBs can lead to electron transport within the internal ASSLBs and cause serious self-discharge as a result. However, the self-discharge issue has been overlooked. Up to now, approaches to tailor the electronic conductivity of GBs to suppress Li dendrites and battery self-discharge are still challenging and sparse.

Here, we propose a grain-boundary electronic insulation (GBEI) strategy to tailor the GBs of Li_6PSCl_5 (LPSCl), a representative HVMEFS-SSE, with an electronically insulating SPE for Li dendrite and self-discharge suppression. Generally, the GBEI-based LPSCl possesses three advantages. As illustrated in **Scheme 1a~c**, firstly, the SPE can transport the Li^+ smoothly while blocking the electron transport at the GBs, which helps suppress Li dendrite growth. Secondly, the limited electron transport in the bulk LPSCl is also beneficial for suppressing self-discharge and enhancing cycling stability. Lastly, the SPE covered on the surface of LPSCl functions as a protection layer to separate the LPSCl and moisture, which improves humidity stability. As proof of the concept, the Li-Li symmetric cell using GBEI-based LPSCl performed stable cycling for over 1000 h at 0.5 mA cm^{-2} (each half cycle of 2 h), whose cycling life was over 30 times of the cell using unmodified LPSCl. Such strong Li dendrite suppression capability enabled stable Li-$LiCoO_2$ (LCO) full cells performance for over 2600 cycles at 0.5 mA cm^{-2}. Moreover, GBEI-based LPSCl showed better anti-humidity performance with an ionic conductivity decay rate three times slower than the unmodified LPSCl. Additionally, the full cells using GBEI-based LPSCl rested at the fully charged state for one week can still deliver a high Coulombic efficiency of 96.1%, which is 8% higher than its counterpart, highlighting the self-discharging suppressing function of the GBEI strategy.

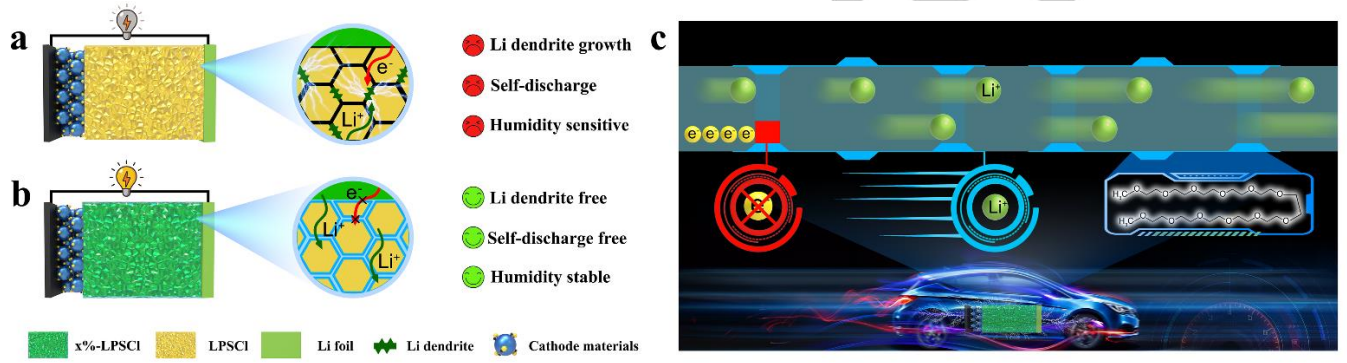

Scheme 1. Schematic illustrations of ASSLBs using (a) LPSCl and (b) x-LPSCl as electrolytes and their different performance on Li dendrite suppression, self-discharge suppression and humidity resistance. **(c)** The schematic shows the role of PEGDME played in the GBEI strategy.

Results and Discussion

In principle, the electronic insulation materials chosen for GBs modification should have the following two features. 1) The materials should possess a relatively high ionic conductivity and an extremely low electronic conductivity, which allow smooth Li^+ transport through the SSE but inhibit electrons accumulation at the GBs. 2) The decoration materials should be chemically stable with LPSCl in order to maintain the high ionic conductivity of LPSCl. With these in mind, a poly(ethylene glycol) dimethyl ether (PEGDME) SPE is chosen as the decoration material to modify the GBs of LPSCl, where PEGDME SPE shows a decent room-temperature ionic conductivity of 5×10^{-6} S cm^{-1} and an extremely low electronic conductivity of 8.39×10^{-11} S cm^{-1} (**Figure S1**).[12] It has great potential to achieve smooth Li^+ transport and block electrons accumulation at GBs concurrently. Moreover, as shown in the X-ray diffraction (XRD) patterns and Raman spectra (**Figure S2**), the mixtures of LPSCl and PEGDME SPE presented unchanged characteristic XRD peaks and Raman bands of LPSCl without any impurity peaks, indicating the high chemical stability between PEGDME SPE and LPSCl. Therefore, the PEGDME SPE can be a promising candidate for GBs modification.

The physical and chemical properties of LPSCl with different contents of PEGDME SPE at the GBs were investigated. The PEGDME SPE was introduced to modify the GBs via a ball-milling method and the PEGDME content was controlled in a range of 0 to 10 wt.%, which is labeled as x-LPSCl (x indicates the weight content of SPE). The morphologies of x-LPSCl are shown in **Figure 1a-d** and **Figure S3**. The pristine LPSCl powders presented a uniform particle size distribution in the range of 50~100 nm. After the introduction of PEGDME SPE, the morphology of the LPSCl particles showed negligible change but gradually appeared to be covered by PEGDME SPE. When the x-LPSCl was pressed into a pellet, the PEGDME SPE further filled in the GBs among LPSCl particles to ensure smooth Li^+ transport and electronic insulation at the GBs. The PEGDME SPE content of 5 wt.% demonstrated full coverage of all the LPSCl particles (**Figure 1c, Figure S3c, g**) and the thickness of PEGDME SPE is determined to be 5~10 nm in the cryo-transmission electron microscopy (cryo-TEM, **Figure 1e-f**). It is worth noting that the PEGDME SPE also filled the GBs between the two LPSCl particles, which is of significance to blocking electron transport at GBs. The uniform distribution of the PEGDME SPE is further evidenced by the high-angle annular dark-field image (HAADF) and elemental mappings in **Figure 1g-l** and **Figure S4**. Further increase in the PEGDME SPE content led to local aggregation, as displayed in **Figure 1d** and **Figure S3d, h** which would adversely affect the ionic conductivity. The ionic and electronic conductivities of the different x-LPSCl composites were evaluated and compared in **Figure 1m-n** and **Figure S5-S6**. Due to the involvement of low-ionic/electronic-conductivity PEGDME SPE, both the ionic conductivity and the electronic conductivity of x-LPSCl showed decreasing tendencies with the increasing PEGDME SPE contents. With the PEGDME SPE content increasing from 0 to 10 wt.%, the ionic conductivity of x-LPSCl acceptably decreased from 1.81 mS cm^{-1} to 0.42 mS cm^{-1}. Nyquist plots of the impedance of x-LPSCl during ionic conductivity testing at 25 °C were shown in **Figure S7**. The spectra were fitted by the equivalent circuit shown in the inset of **Figure S7b**. The semicircle and the intersection between the semicircle and the x-axis reflected

10.1002/anie.202215680

the impedance of GBs and grains, respectively. [13] As can be seen, the impedance of grains remained roughly 40 Ω, while the grain boundary impedance increased sharply from 15.2 Ω to 170.9 Ω with PEGDME SPE content increasing from 0 wt.% to 10 wt.%, further proving the successful introduction of PEGDME SPE in GBs. It is worth mentioning that the modification of GBs with PEGDME SPE dramatically reduced the electronic conductivity by 26 times from 5.79×10^{-8} S cm^{-1} to 2.2×10^{-9} S cm^{-1}. On one hand, the lower electronic conductivity can help to suppress Li dendrite growth and self-discharge; on the other hand, the lower ionic conductivity would lead to increased polarization and worse rate capability. Therefore, the PEGDME SPE content should be carefully optimized by balancing trade-offs between ionic conductivity and electronic conductivity.

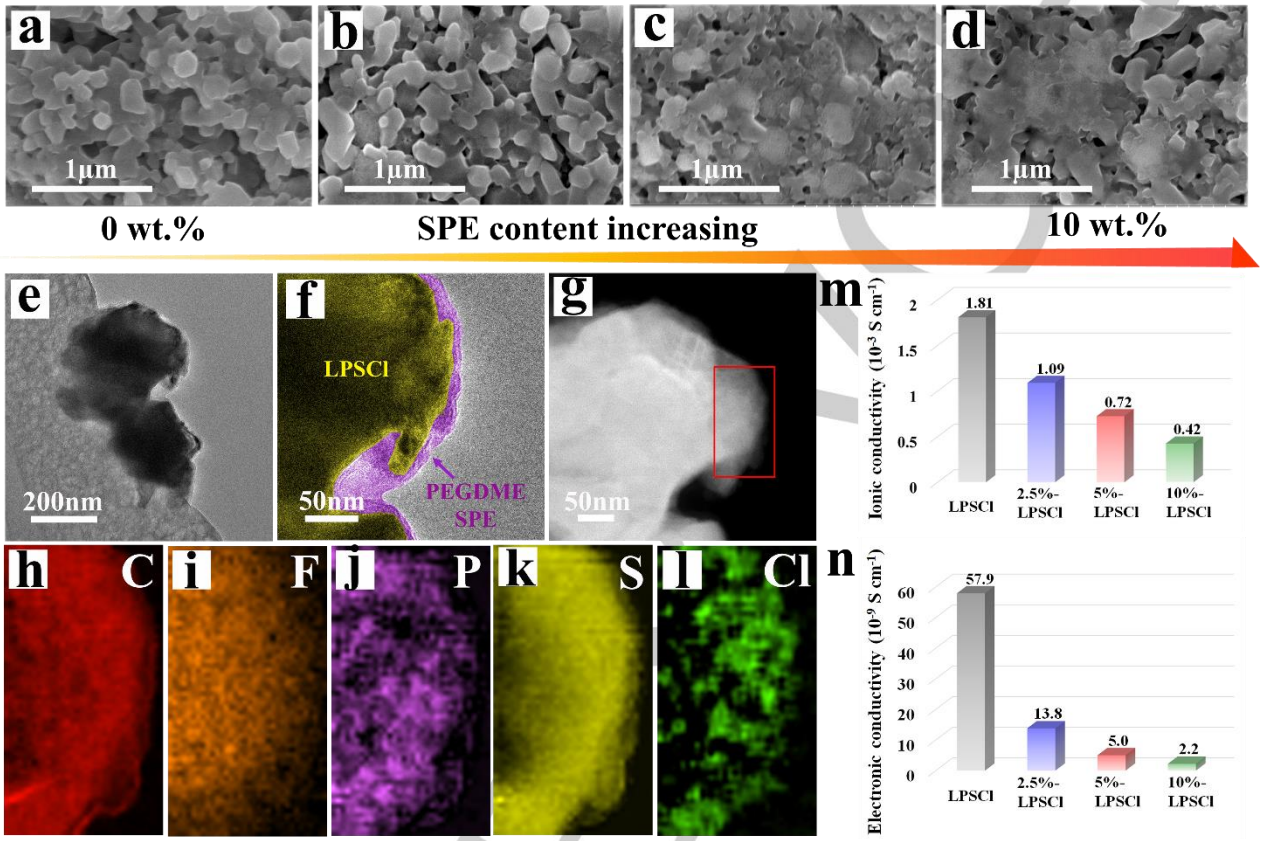

Figure 1. SEM images of x-LPSCl with different SPE contents of (**a**) 0 wt.%, (**b**) 2.5 wt.%, (**c**) 5 wt.%, (**d**) 10 wt.%. (**e-f**) TEM images, (**g**) High-angle annular dark-field image (HAADF) and electron energy loss spectroscopy (EELS) mapping on the elemental distribution of (**h**) C, (**i**) F, (**j**) P, (**k**) S, (**l**) Cl. (**m**) Ionic conductivities and (**n**) electronic conductivities of x-LPSCl.

The effect of the GBEI strategy on Li dendrite suppression was studied. For the Li-Li symmetric cell using pristine LPSCl SSE, stable Li plating/stripping performance was observed at relatively low current densities of 0.1 mA cm^{-2} and 0.25 mA cm^{-2} with an areal capacity of 0.5 mAh cm^{-2} (**Figure S8**) for over 1000 h. However, when the current density increased to 0.5 mA cm^{-2}, the cell had a short circuit in less than 50 h. The difference in cycling stability can be attributed to different Li deposition models. At low current densities, the GBs potential can remain above 0 V, where fresh Li was preferentially deposited at the interface between the Li metal electrode and the SSE pellet. In contrast, a current density of 0.5 mA cm^{-2} was large enough to reduce the GBs potential to below 0 V. In this case, the GBs served as the channels for Li deposition.[11] The continuous Li deposition and Li dendrite growth along the GBs eventually resulted in a short circuit (as illustrated in **Figure 2a**). Further increasing the capacity to 1 mAh cm^{-2}, the Li-Li symmetric cell using LPSCl SSE can only run for 30 h before a short circuit occurred (**Figure 2c**). The occurrence of a short circuit was confirmed by ex-situ electrochemical impedance spectroscopy (EIS) and scanning electronic microscopy (SEM) images. As shown in **Figure S9a**, the cell resistance was increased during the first few cycles, which can be attributed to the interfacial reactions between Li and LPSCl and interphase formation.[14] A sudden decrease in resistance was observed by the EIS results at the 10th and 20th cycles, suggesting the occurrence of a short circuit, which coincided with the sudden drop of overpotentials for plating/stripping profiles in **Figure 2c**.[15] The SEM images of the LPSCl pellet cross-section after 20 cycles (80 h) are displayed in **Figure 2j** and **Figure S10a-c**. Similar to previous reports, metallic Li was detected within the bulk SSE pellet, which was evidenced by the uneven elemental mappings of P, S and Cl as shown in **Figure 2k-m**.[8b, 8c, 16] The Li deposition in bulk LPSCl can be attributed to the reduction of Li^+ by electrons at the GBs.[11] In contrast, the introduction of PEGDME SPE blocked the electron transport at GBs, the Li dendrite growth in bulk LPSCl was greatly suppressed and the cycling life of Li-Li symmetric cells was prolonged (**Figure 2b-c**). Especially, the Li-Li symmetric cells using 5%-LPSCl and 10%-LPSCl SSEs presented stable Li plating/stripping behavior for over 1000 h, which was over 30 times their counterpart without PEGDME SPE modification. The electrochemical performance of Li-Li symmetric cells is superior to most recent reports based on Li/SSE interface design and elemental doping for sulfide SSE modification, as shown in **Figure S11** and **Table S1**.[6b, 6c, 7a, 17] For the Li-Li symmetric cells assembled with 2.5 %-LPSCl, a short circuit is still observed after 170 h. The 2.5 wt.% SPE was probably not sufficient to completely cover

10.1002/anie.202215680

all the LPSCl particles and fill all the GBs (**Figure 1b** and **Figure S3b, f**), thus Li dendrite growth may occur at the unprotected GBs. On the other hand, raising the SPE content led to a gradual increase in overpotential from 39 mV (LPSCl) to 115 mV (10%-LPSCl) due to the reduced ionic conductivity, which can be detrimental to high-rate capability (**Figure S12**). Overall, the 5%-LPSCl composite SSE showed an optimized balance between overpotential and cycling life. The corresponding EIS results during cycling (**Figure S9b**) and the SEM morphology of the 5%-LPSCl SSE pellet after 250 cycles (1000 h) (**Figure 2d-i**, and **Figure S10d-f**) confirmed the high stability and Li dendrite-free behavior of the 5%-LPSCl. As shown in **Figure S9b**, the slight increase in cell resistance during the first few cycles reflected the SEI formation process at the Li/SSE interface, but the stabilized resistance after 10 cycles supported the stable Li plating/stripping behavior. [18] Even after long-term plating/stripping for over 1000 h, no metallic Li is detected in the bulk 5%-LPSCl pellet (**Figure 2d-i**, and **Figure S10d-f**). The critical current density (CCD) was further applied to investigate the different capabilities of the Li-Li symmetric cell using LPSCl and 5%-LPSCl SSEs in Li dendrite suppression. [19] The current densities were increased from 0.1 mA cm^{-2} to 2 mA cm^{-2} and each half cycle is 1 h. **Figure S13** showed that the CCD of the Li-Li symmetric cell using 5%-LPSCl SSE is 1.5 mA cm^{-2}, which is much higher than that of LPSCl SSE with a CCD of 0.8 mA cm^{-2}. The CCD and areal capacity of the Li-Li symmetric cell using 5%-LPSCl SSE is superior to most recently reported relying on doping and interface modification strategies listed in **Figure S14** and **Table S2**.[17g, 17i, 20] The huge difference in Li plating-stripping behavior before and after GBs modification with PEGDME SPE further highlights the positive effect of the GBEI strategy on suppressing Li dendrite growth.

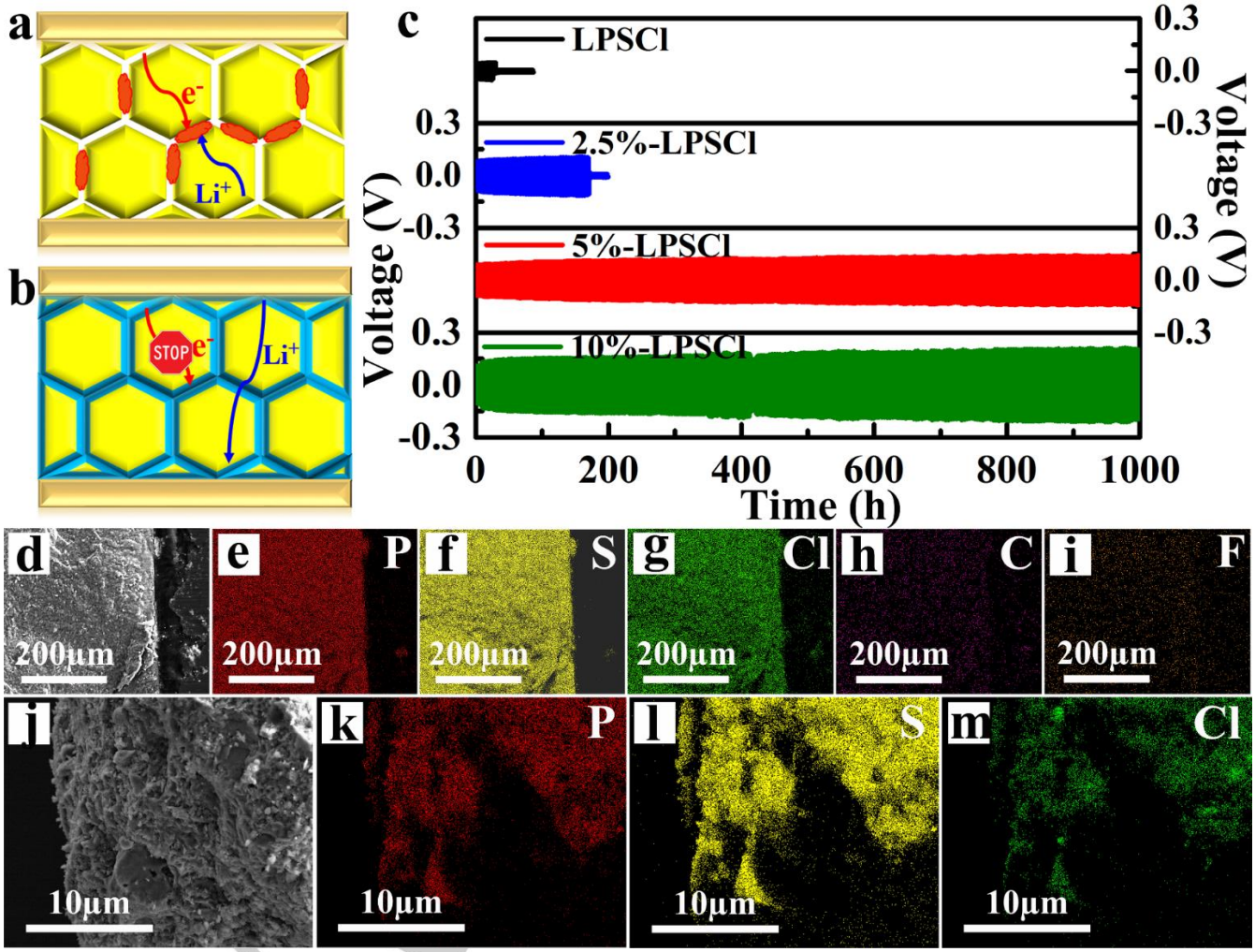

Figure 2. Schematic illustrations showing different ionic/electronic conducting behaviors of (**a**) LPSCl and (**b**) x-LPSCl SSEs for Li dendrite suppression. (**c**) The cycling performance of Li-Li symmetric cells using x-LPSCl (x = 0-10%) at a current density of 0.5 mA cm^{-2} and an areal capacity of 1 mAh cm^{-2}. (**d**) Cross-sectional SEM image of the 5%-LPSCl pellet after 250 cycles and the corresponding elemental mappings of (**e**) P, (**f**) S, (**g**) Cl, (**h**) C and (**i**) F. (**j**) Cross-sectional SEM image of the LPSCl pellet after 20 cycles and the corresponding elemental mappings of (**k**) P, (**l**) S, (**m**) Cl.

To clarify the underlying mechanism of the GBEI strategy for blocking electron transport at GBs, the DFT calculation results including the electrostatic potential profiles and projected density of states (PDOS) are shown in **Figure 3** for Li(100)/LPSCl(100), Li(100)/PEGDME and LPSCl(100)/PEGDME (**Figure S15** and **Figure 3a-c**), respectively. In the case of Li(100)/LPSCl(100), there was no electron tunneling barrier for the electrons transfer from the Li interface to the LPSCl (**Figure 3d**), where Li^+ is easily reduced by the electrons in LPSCl and referentially deposits in LPSCl rather than at Li/LPSCl interface. [17a, 19a] The behavior was further supported by PDOS results, as shown in **Figure 3g**. The Li/LPSCl interface was

10.1002/anie.202215680

found highly electronic conductive and failed to block the migration of electrons from the Li metal anode to the inner LPSCl, resulting in Li dendrite growth through the LPSCl SSE.

In the case of GBEI-based LPSCl, the PEGDME directly contacted the Li metal anode and filled in the GBs to separate the LPSCl particles. Therefore, the electrostatic potential profiles and PDOS simulation results were evaluated based on the relaxed Li(100)/PEGDME model. Due to the electronically insulating nature of PEGDME indicated by its separate PDOS (**Figure 3h**), the electrostatic potential of the Li/PEGDME interface was determined to be 2.07 eV lower than that within the PEGDME polymer (**Figure 3e**). In other words, transferring electrons from the Li/PEGDME interface to bulk PEGDME would be required to overcome an energy barrier of 2.07 eV. In this case, Li deposition preferentially occurs at the interface rather than within the PEGDME, inhibiting Li dendrite penetration through the GBEI-based LPSCl. [19a] Even if some unprotected LPSCl particles were to contact the Li metal anode at the SSE/anode interface, electrons can migrate from the Li/LPSCl interface into the superficial LPSCl particle but be blocked by the electronically insulating PEGDME at the GBs (**Figure 3i**). The electron tunneling barrier was determined as 0.74eV from the LPSCl/PEGDME interface to PEGDME (**Figure 3f**). Therefore, as long as the GBs of LPSCl are modified with sufficient PEGDME SPE, the electronic transfer can be blocked by the surface PEGDME coverage and the GBs filling PEGDME, and Li dendrite growth in the bulk GBEI-based LPSCl can be prohibited.

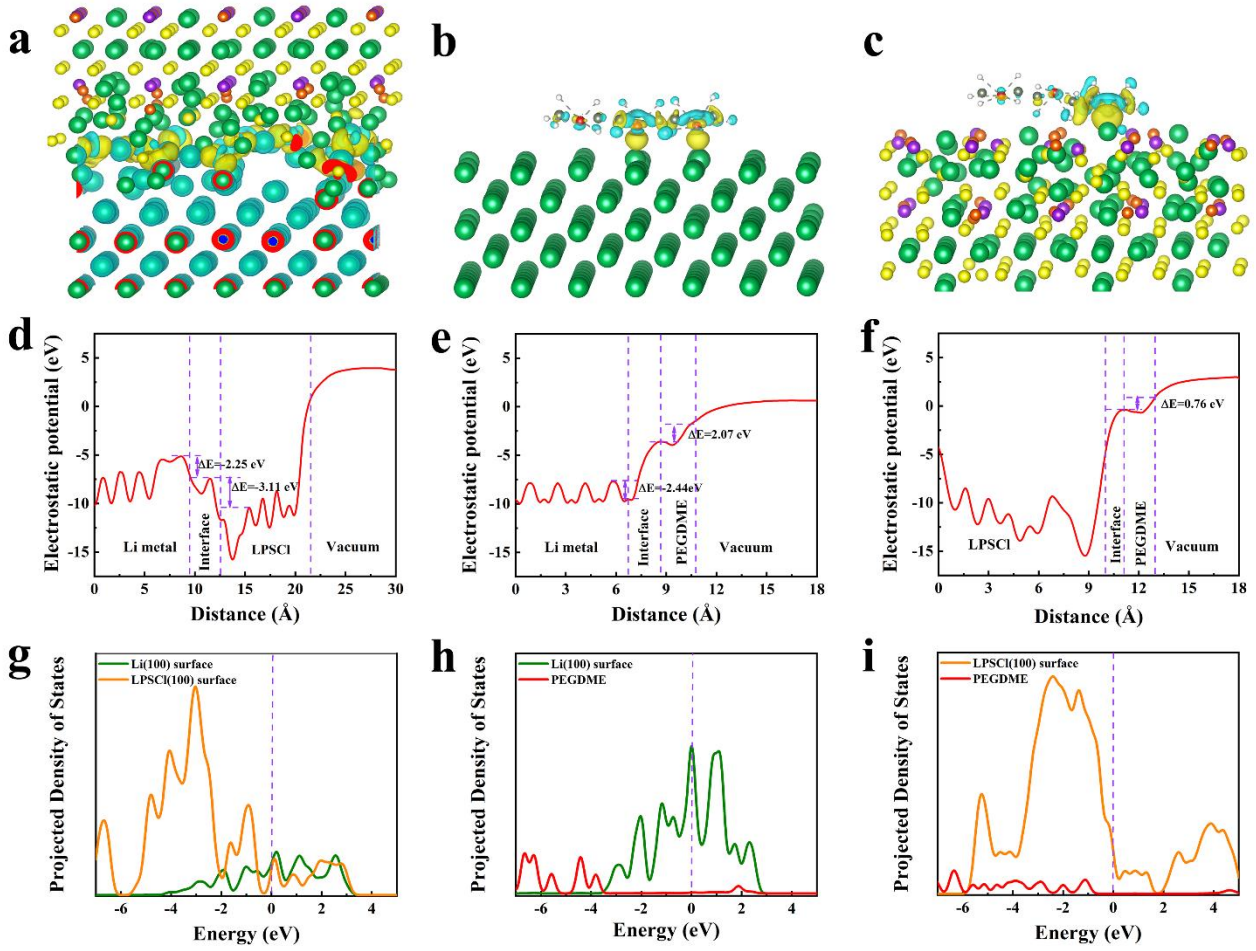

Figure 3. The structure and charge density difference of (**a**) Li(100)/LiPSCl(100), (**b**) Li(100)/PEGDME and (**c**) LiPSCl(100)/PEGDME. The electrostatic potential profiles of (**d**) Li(100)/LiPSCl(100), (**e**) Li(100)/PEGDME and (**f**) LiPSCl(100)/PEGDME. The PDOS of (**g**) Li(100)/LiPSCl(100), (**h**) Li(100)/PEGDME and (**i**) LiPSCl(100)/PEGDME.

In addition to the concern of Li dendrite growth along the GBs, the poor humidity stability is another limitation for sulfide SSEs.[2b, 21] To examine the effect of PEGDME SPE modification on the humidity stability for LPSCl, both LPSCl and 5%-LPSCl were exposed to air with 3% humidity for 10 h (labeled as LPSCl-exposure and 5%-LPSCl-exposure, respectively). After exposure, as shown in **Figure 4a**, the ionic conductivity of LPSCl at 25 °C decreased from 1.81 to 0.32 mS cm^{-1}, showing ionic conductivity retention of roughly 18%. In comparison, after the same exposure treatment, the ionic conductivity of the 5%-LPSCl was less affected (**Figure 4b**). The ionic conductivity at 25 °C was only lowered from 0.72 to 0.39 mS cm^{-1}, corresponding to ionic conductivity retention of 54%. The SPE protection can reduce the humidity-induced decay rate of ionic conductivity by three times. The chemical evolution of LPSCl during its exposure to moisture was characterized by XRD and X-ray photoelectron spectroscopy (XPS). As shown in **Figure 4c**, similar impure phases were observed on the XRD patterns of both LPSCl-exposure and 5%-LPSCl-exposure samples due to reactions with moisture.[22] The reduced peak intensity of impurity phases with the coverage of PEGDME SPE highlighted its effect on improving humidity stability, which was consistent with better ionic conductivity retention after moisture exposure. More chemical information was revealed by XPS, as exhibited in **Figure 4d-e** and **Figure S16**. Considering the decomposition of LPSCl mainly results from the unstable PS_4^{3-} tetrahedra, [23] the S 2p and P 2p spectra were

10.1002/anie.202215680

obtained. The S 2p and P 2p spectra are doublets comprised of closely spaced spin-orbit components due to $2p_{3/2}$ and $2p_{1/2}$. Each S- and P-containing species consistently exhibited pairs of characteristic doublets, so only the intensity of the $2p_{3/2}$ peak will be discussed in the following discussion for simplicity. Before air exposure, the P $2p_{3/2}$ peak at 131.9 eV and the S $2p_{3/2}$ peak at 161.4 eV in the spectra were assigned to PS_4^{3-} of LPSCl, [24] whereas the peak at roughly 169 eV in the S 2p spectra of 5%-LPSCl was attributed to the sulfonyl group from the lithium bis(trifluoromethanesulfonyl)imide (LiTFSI) salt (**Figure S17**). After moisture exposure, a pair of new peaks appeared at around $2p_{3/2}$ of 132.8 eV in P 2p spectra, which was attributed to the substitution of S in PS_4^{3-} by O and the formation of PO_xS_y (**Figure 4d-e**). [25] In the S 2p spectra, the appearance of sulfate at approximately 169.0 eV and sulfite at 166.9 eV further confirmed the oxidization of LPSCl (**Figure S16**).[26] Notably, the peak intensity of the side products (PO_xS_y, sulfate, and sulfite) in the 5%-LPSCl-exposure spectra was much weaker than that of the LPSCl-exposure. The weakened peak intensity of side products highlighted the improved humidity stability with the assistance of PEGDME SPE. The function of PEGDME SPE on improving the humidity stability for LPSCl is illustrated in **Figure 4f**. The coverage of PEGDME SPE on the surface of LPSCl inhibited the direct contact between LPSCl and moisture, which hindered the decomposition of PS_4^{3-} tetrahedra, thus reducing the side product formation (**Figure 4c**) and maintaining good ionic conductivity retention (**Figure 4b**). Improving humidity stability is critical for sulfide SSEs storage and sulfide SSE-based electrode preparation in the dry room for practical application.

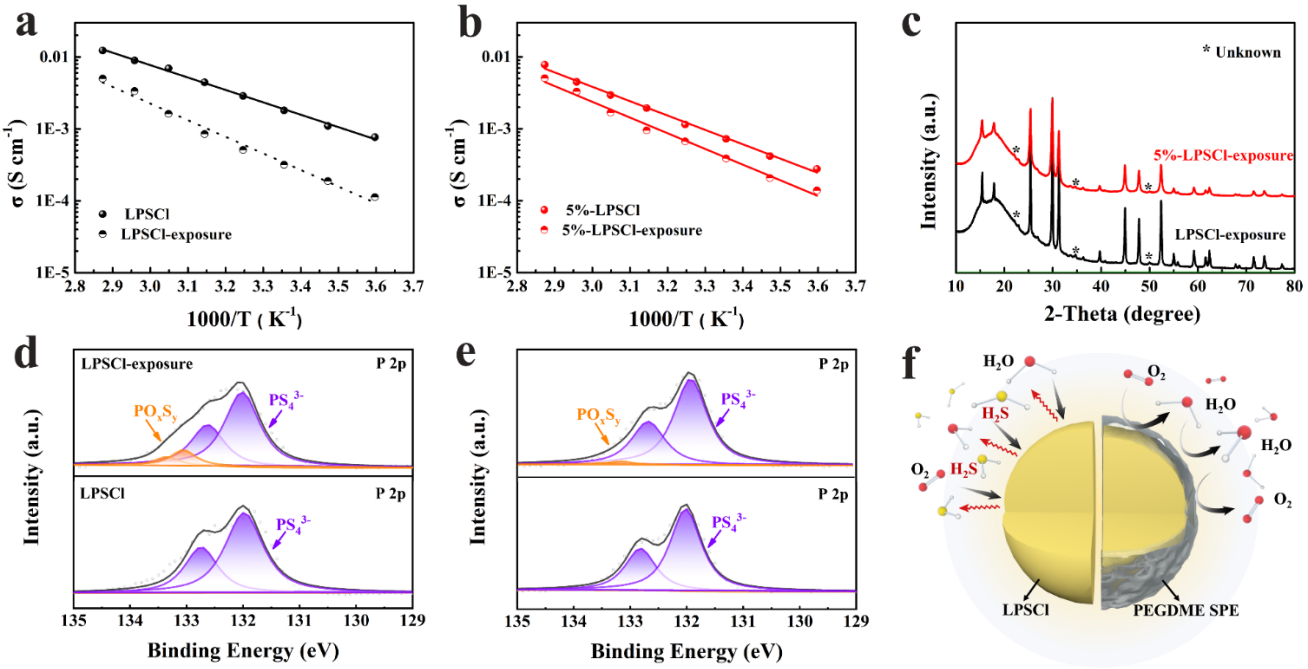

Figure 4. The ionic conductivities of (**a**) LPSCl and LPSCl-exposure and (**b**) 5% LPSCl and 5%-LPSCl-exposure samples. (**c**) XRD patterns of LPSCl-exposure and 5%-LPSCl-exposure samples. P 2p XPS spectra of (**d**) LPSCl and LPSCl-exposure and (**e**) 5%-LPSCl and 5%-LPSCl-exposure samples. (**f**) Schematic illustration of the protection of PEGDME SPE on improving the humidity stability of LPSCl SSE.

As we discussed earlier, the non-negligible electronic conductivity of HVMEFS-SSEs can lead to Li dendrite growth along the GBs and result in serious self-discharge. Comprehensive effects of the different Li dendrite and self-discharge suppressing capabilities of LPSCl and 5%-LPSCl SSEs were evaluated and verified by the electrochemical performance of Li-LCO full-cell ASSLBs (**Figure 5a**). The LCO cathode materials were protected by a $LiZrO_x$ (LZO) coating layer to hinder the interfacial side reactions between LCO and x-LPSCl.[27] The LZO-coated LCO cathode material is named LZO@LCO. The cycling performance of Li-LCO ASSLBs using LPSCl and 5%-LPSCl SSEs (labeled as Li/LPSCl/LZO@LCO and Li/5%-LPSCl/LZO@LCO, respectively) were tested at a galvanostatic charge/discharge current density of 0.1 mA cm^{-2} between 2.5 V and 4.2 V. As can be seen, the Li/5%-LPSCl/LZO@LCO delivered a high initial capacity of 130 mAh g^{-1}, which is 5 mAh g^{-1} lower than that of Li/LPSCl/LZO@LCO cell. The reduced capacity is mainly due to the reduced ionic conductivity relying on the GBEI strategy that reduced the electrochemical kinetics. It is further proved by the EIS results in **Figure S18**, where the Li/5%-LPSCl/LZO@LCO cell performed a higher charge transfer resistance (R_{ct}) of 66.6 Ω compared with Li/LPSCl/LZO@LCO cell (29.7 Ω). For the self-discharging study, cells were initially cycled for three cycles to reach a stable state with high Coulombic efficiencies (CEs) of 98.6% for Li/LPSCl/LZO@LCO and 99.7% for Li/5%-LPSCl/LZO@LCO, respectively (**Figure S19**). After pre-conditioning, the cells were charged to 4.2 V and then left at rest for one week (168 h) to evaluate the self-discharge rate of cells using the two different SSEs. As displayed in **Figure 5b-c**, the Li/LPSCl/LZO@LCO cell delivered a relatively low CE of 88.1%, indicating the serious self-discharge behavior with 10.5% CE drop due to the non-negligible electronic conductivity of LPSCl. On the contrary, thanks to the GBEI strategy on electron-blocking, Li/5%-LPSCl/LZO@LCO cell delivered a high capacity retention of 96.1%, indicating 3 times lower self-discharging rate with the assistance of the GBEI strategy (3.6% vs. 10.5%). The improved self-discharging suppression capability of the GBEI strategy is further evidenced by the voltage curves during the standing period. As shown in **Figure S20**, the voltage of Li/5%-LPSCl/LZO@LCO dropped much slower than that of Li/LPSCl/LZO@LCO, indicating a slower self-discharging rate. During the long-term cycling of 350 cycles (except the first 4 cycles), the Li/5%-LPSCl/LZO@LCO cell performed a high average

10.1002/anie.202215680

CE of 99.7%. It was 1.2% higher than its counterpart (Li/LPSCl/LZO@LCO, 98.5%), which further highlighted the positive effect of the GBEI strategy on alleviating self-discharge in sulfide-based ASSLBs.

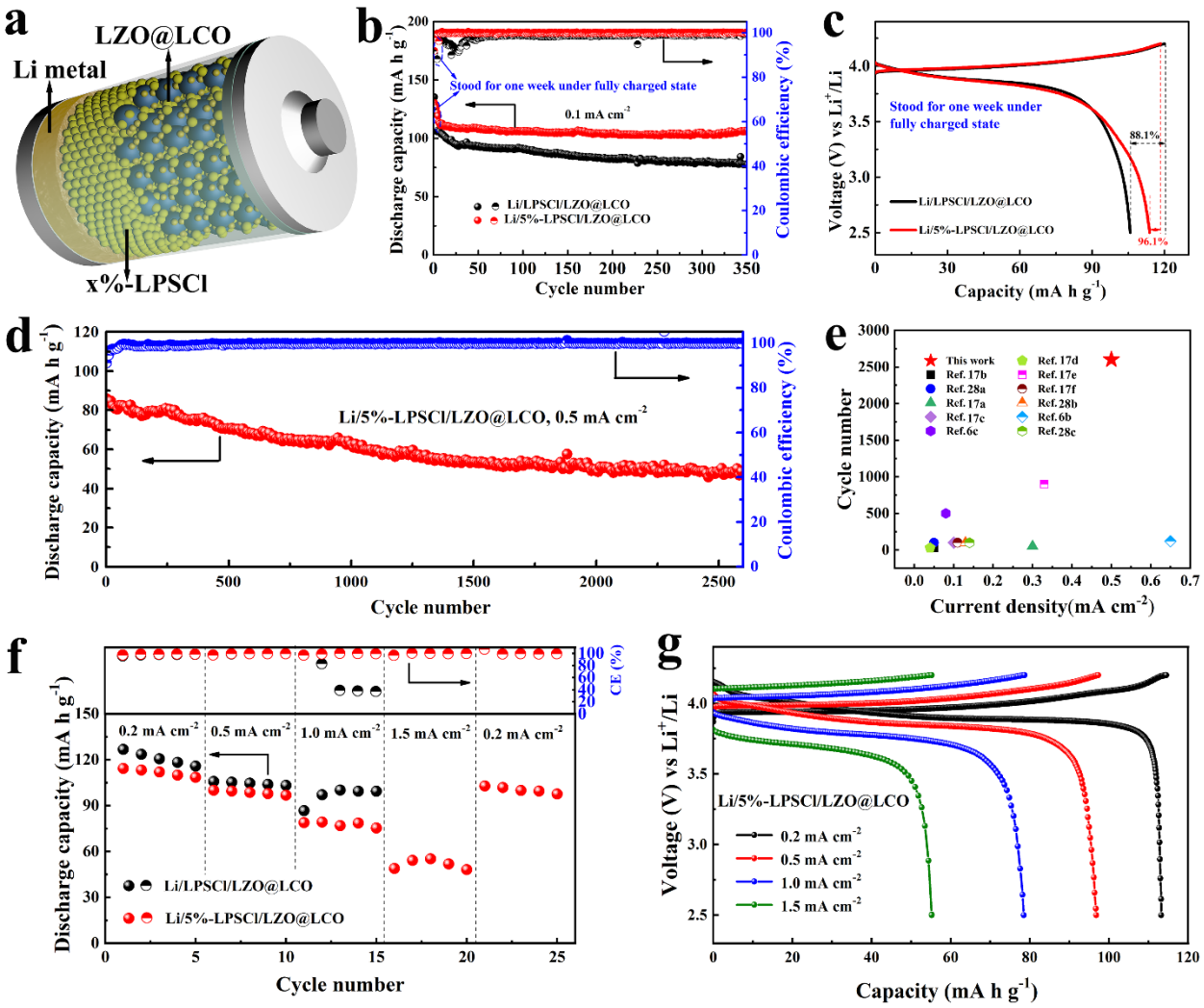

Figure 5. (**a**) Schematic illustration of an ASSLB using x-LPSCl as electrolyte and LZO@LCO as cathode active material. (**b**) Cycling performance of Li/LPSCl/LZO@LCO and Li/5%-LPSCl/LZO@LCO cells at 0.1 mA cm^{-2}; the cells were rested at the fully charged state at the 4th cycle for one week to evaluate their self-discharging effects on (**c**) charging-discharging profiles. (**d**) Long-term cycling performance of the Li/5%-LPSCl/LZO@LCO cell at 0.5 mA cm^{-2} and (**e**) Comparison of the recently reported full cells using sulfide SSEs with respect to current density and cycling life. (**f**) Rate performance of Li/LPSCl/LZO@LCO and Li/5%-LPSCl/LZO@LCO cells at various current densities from 0.2 mA cm^{-2} to 1.5 mA cm^{-2}. (**g**) Charging-discharging profiles of Li/5%-LPSCl/LZO@LCO cell at various current densities.

The different Li dendrite suppression capabilities of LPSCl and 5%-LPSCl made a difference in the cycling performance of Li/LPSCl/LZO@LCO and Li/5%-LPSCl/LZO@LCO cells at a current density of 0.5 mA cm^{-2}. As shown in **Figure S21a**, a short circuit occurred in the Li/LPSCl/LZO@LCO cell at as early as the 8th cycle, where the CE dramatically dropped from 99.7% to 15.2 % with a significantly extended charging process. The occurrence of a short circuit was further confirmed by the charge/discharge profiles (**Figure S21b**). The LPSCl alone did not meet the demand of Li dendrite suppression for Li-LCO cells. On the contrary, consistently high CEs of around 100% with no short circuit phenomenon were observed for the Li/5%-LPSCl/LZO@LCO cell during the long-term cycling. The assembled cells delivered a high capacity retention of 80% at 650 cycles and stable cycling performance for over 2600 cycles at 0.5 mA cm^{-2} (**Figure 5d** and **Figure S22**). Such long cycling performance of Li-LCO ASSLBs has surpassed the most recent reports as listed in **Table S3** and **Figure 5e**.[6b, 6c, 17a-f, 28] Additionally, the rate capability of Li/LPSCl/LZO@LCO and Li/5%-LPSCl/LZO@LCO cells were investigated at various current densities from 0.2 mA cm^{-2} to 1.5 mA cm^{-2}. As shown in **Figure 5f~g** and **Figure S23**, the Li/5%-LPSCl/LZO@LCO cell delivered a capacity of over 55 mAh g^{-1} at a high current density of 1.5 mA cm^{-2} and no short circuit was observed. The results coincided well with the CCD results in **Figure S13** and further highlighted the improved capability in dendrite suppression relying on the GBEI strategy. In contrast, a sharply decreasing in CE from 99.5% (10th cycle, 0.5 mA cm^{-2}) to 39.1% (13th cycle, 1.0 mA cm^{-2}) for Li/LPSCl/LZO@LCO indicated the occurrence of a short circuit, which is further proved by the charging-discharging profiles in **Figure S23**. To further explore the potential of the GBEI strategy in practical application, the cycling stability of Li/5%-LPSCl/LZO@LCO assembled with a 22.4 mg cm^{-2} LCO-loaded cathode was studied. As displayed in **Figure S24**, the cell delivered a high capacity of 106 mAh g^{-1} at 0.2 mA cm^{-2} after activation at 0.1 mA cm^{-2} for 1 cycle, corresponding to a high areal capacity of ~2.4 mAh cm^{-2}. Moreover, the cell can stably run for over 80 cycles and maintained a high areal

capacity of ~1.6 mAh cm^{-2} (**Figure S24b**), showing great potential in practical application. The huge differences between LPSCl and 5%-LPSCl in Li dendrite/self-discharging suppression and humidity stability highlighted the importance of the GBEI strategy in pursuing long-cycling-life ASSLBs.

Conclusion

In summary, we proposed a GBEI strategy for Li dendrite and self-discharge suppression via tailoring the GBs with a low-electronic-conductivity PEGDME SPE. The electronically insulating nature of the PEGDME SPE can block the electron transport at the GBs, thus inhibiting Li^+ reduction by electrons to Li metal at GBs. As a result, Li-Li symmetric cells using GBEI-based LPSCl presented stable plating/stripping behaviors for over 1000 h at 0.5 mA cm^{-2} and 1 mAh cm^{-2}, extending the cycling life by over 30 times compared with cells using pristine LPSCl. Beneficial from the limited electron transport through the GBEI-based LPSCl, the assembled Li-LCO ASSLBs maintained a high capacity retention of 96.1% after standing for one week at a fully charged state. It was 8% higher than its counterpart. Based on the unique GBEI properties, the Li-LCO ASSLBs delivered a high capacity retention of 80% at 650 cycles and stable cycling performance for over 2600 cycles at 0.5 mA cm^{-2}. In addition to the improved Li dendrite and self-discharge suppressing capabilities, the coverage of SPE can also protect the LPSCl from moisture, thus improving the humidity stability and presenting a three times lower ionic conductivity decay rate. This work represents the tailoring electronic conductivity of GBs, and presents a promising strategy to achieve dendrite- and self-discharge-free and humidity-stable ASSLBs.

Acknowledgements

This work was partly supported by the Natural Sciences and Engineering Research Council of Canada (NSERC), Canada Research Chair Program (CRC), Canada Foundation for Innovation (CFI), Ontario Research Fund, China Automotive Battery Research Institute Co., Ltd, Glabat Solid-State Battery Inc. and University of Western Ontario. C. V. Singh acknowledges additional support from Hart Professorship, Compute Canada, and the University of Toronto.

Statement of Contributions

X. Yang, X. Gao and M. Jiang contributed equally to this work. X. Yang and X. Gao conceived and designed the experimental work and prepared the manuscript; X. Gao helped with SEM characterization, J. Yan and Y. Tang helped with cryo-TEM testing and analysis; M. Fu helped with XRD testing and analysis; M. Jiang, and C. V. Singh designed and performed DFT calculations and analysis; J. Luo, H. Duan, S. Zhang, R. Yang and H. Huang participated in the discussion of the data; R. Li purchased all the chemicals; J. Wang, H. Huang, X. Sun supervised the overall project. All authors have approved the final version of the manuscript.

Keywords: All-solid-state lithium batteries; • Grain Boundaries • Lithium dendrite • Self-discharging • Humidity stability

[1] a) R. Chen, Q. Li, X. Yu, L. Chen, H. Li, *Chem. Rev.* **2019**, 120, 6820; b) C. Wang, K. Fu, S. P. Kammampata, D. W. McOwen, A. J. Samson, L. Zhang, G. T. Hitz, A. M. Nolan, E. D. Wachsman, Y. Mo, V. Thangadurai, L. Hu, *Chem. Rev.* **2020**, 120, 4257; c) A. Manthiram, X. Yu, S. Wang, *Nat. Rev. Mater.* **2017**, 2, 16103; d) X. Yang, J. Luo, X. Sun, *Chem. Soc. Rev.* **2020**, 49, 2140; e) Y. Pang, J. Pan, J. Yang, S. Zheng, C. Wang, *Electrochem. Energy Rev.***2021**, 4, 169.

[2] a) C. Wang, J. Liang, Y. Zhao, M. Zheng, X. Li, X. Sun, *Energy Environ. Sci.* **2021**, 14, 2577; b) C. Yu, F. Zhao, J. Luo, L. Zhang, X. Sun, *Nano Energy* **2021**, 83, 105858; c) J. Wu, L. Shen, Z. Zhang, G. Liu, Z. Wang, D. Zhou, H. Wan, X. Xu, X. Yao, *Electrochem. Energy Rev.* **2020**, 4, 101.

[3] a) N. Kamaya, K. Homma, Y. Yamakawa, M. Hirayama, R. Kanno, M. Yonemura, T. Kamiyama, Y. Kato, S. Hama, K. Kawamoto, A. Mitsui, *Nat. Mater.* **2011**, 10, 682; b) P. Bron, S. Johansson, K. Zick, J. Schmedt auf der Gunne, S. Dehnen, B. Roling, *J. Am. Chem. Soc.* **2013**, 135, 15694.

[4] a) M. R. Busche, D. A. Weber, Y. Schneider, C. Dietrich, S. Wenzel, T. Leichtweiss, D. Schröder, W. Zhang, H. Weigand, D. Walter, S. J. Sedlmaier, D. Houtarde, L. F. Nazar, J. Janek, *Chem. Mater.* **2016**, 28, 6152; b) W. D. Jung, J. S. Kim, S. Choi, S. Kim, M. Jeon, H. G. Jung, K. Y. Chung, J. H. Lee, B. K. Kim, J. H. Lee, H. Kim, *Nano Lett.* **2020**, 20, 2303; c) Z. Liu, W. Fu, E. A. Payzant, X. Yu, Z. Wu, N. J. Dudney, J. Kiggans, K. Hong, A. J. Rondinone, C. Liang, *J. Am. Chem. Soc.* **2013**, 135, 975.

[5] S. Wenzel, S. Randau, T. Leichtweiß, D. A. Weber, J. Sann, W. G. Zeier, J. Janek, *Chem. Mater.* **2016**, 28, 2400.

[6] a) L. Ye, X. Li, *Nature* **2021**, 593, 218; b) C. Wang, K. R. Adair, J. Liang, X. Li, Y. Sun, X. Li, J. Wang, Q. Sun, F. Zhao, X. Lin, R. Li, H. Huang, L. Zhang, R. Yang, S. Lu, X. Sun, *Adv. Funct. Mater.***2019**, 29,1900392.; c) Z. Zhang, S. Chen, J. Yang, J. Wang, L. Yao, X. Yao, P. Cui, X. Xu, *ACS Appl. Mater. Interfaces* **2018**, 10, 2556.

[7] a) F. Han, J. Yue, X. Zhu, C. Wang, *Adv. Energy Mater.* **2018**, 8; b) F. Zhao, Q. Sun, C. Yu, S. Zhang, K. Adair, S. Wang, Y. Liu, Y. Zhao, J. Liang, C. Wang, X. Li, X. Li, W. Xia, R. Li, H. Huang, L. Zhang, S. Zhao, S. Lu, X. Sun, *ACS Energy Lett.* **2020**, 5, 1035.

[8] a) K. B. Hatzell, X. C. Chen, C. L. Cobb, N. P. Dasgupta, M. B. Dixit, L. E. Marbella, M. T. McDowell, P. P. Mukherjee, A. Verma, V. Viswanathan, A. S. Westover, W. G. Zeier, *ACS Energy Lett.* **2020**, 5, 922; b) M. Sun, T. Liu, Y. Yuan, M. Ling, N. Xu, Y. Liu, L. Yan, H. Li, C. Liu, Y. Lu, Y. Shi, Y. He, Y. Guo, X. Tao, C. Liang, J. Lu, *ACS Energy Lett.* **2021**, 6, 451; c) J. Kasemchainan, S. Zekoll, D. Spencer Jolly, Z. Ning, G. O. Hartley, J. Marrow, P. G. Bruce, *Nat. Mater.* **2019**, 18, 1105.

[9] L. Porz, T. Swamy, B. W. Sheldon, D. Rettenwander, T. Frömling, H. L. Thaman, S. Berendts, R. Uecker, W. C. Carter, Y. M. Chiang, *Adv. Energy Mater.***2017**, 7, 1701003.

[10] F. Han, A. S. Westover, J. Yue, X. Fan, F. Wang, M. Chi, D. N. Leonard, N. J. Dudney, H. Wang, C. Wang, *Nat. Energy* **2019**, 4, 187.

[11] X. Liu, R. Garcia-Mendez, A. R. Lupini, Y. Cheng, Z. D. Hood, F. Han, A. Sharafi, J. C. Idrobo, N. J. Dudney, C. Wang, C. Ma, J. Sakamoto, M. Chi, *Nat. Mater.* **2021**, 20, 1485.

[12] X. Yang, M. Jiang, X. Gao, D. Bao, Q. Sun, N. Holmes, H. Duan, S. Mukherjee, K. Adair, C. Zhao, j. Liang, W. Li, J. Li, Y. Liu, H. Huang, L. Zhang, S. Lu, Q. Lu, R. Li, C. V. Singh, X. Sun, *Energy Environ. Sci.* **2020**, 13, 1318.

[13] P. Bron, S. Dehnen, B. Roling, Journal of Power Sources **2016**, 329, 530.

[14] a) Y.-W. Byeon, H. Kim, *Electrochem* **2021**, 2, 452; b) B. Chen, C. Xu, H. Wang, J. Zhou, *Curr. Appl. Phys.* **2019**, 19, 149.

[15] a) X. Yang, X. Gao, C. Zhao, Q. Sun, Y. Zhao, K. Adair, J. Luo, X. Lin, J. Liang, H. Huang, L. Zhang, S. Lu, R. Li, X. Sun, *Energy Storage Mater.* **2020**, 27, 198; b) X. Yang, Q. Sun, C. Zhao, X. Gao, K. R. Adair, Y. Liu, J. Luo, X. Lin, J. Liang, H. Huang, L. Zhang, R. Yang, S. Lu, R. Li, X. Sun, *Nano Energy* **2019**, 61, 567.

[16] Z. Ning, D. S. Jolly, G. Li, R. De Meyere, S. D. Pu, Y. Chen, J. Kasemchainan, J. Ihli, C. Gong, B. Liu, D. L. R. Melvin, A. Bonnin, O. Magdysyuk, P. Adamson, G. O. Hartley, C. W. Monroe, T. J. Marrow, P. G. Bruce, *Nat. Mater.* **2021**, 20, 1121.

[17] a) X. Fan, X. Ji, F. Han, J. Yue, J. Chen, L. Chen, T. Deng, J. Jiang, C. Wang, *Sci. Adv.* **2018**, 4, eaau9245; b) Y. Tao, S. Chen, D. Liu, G. Peng, X. Yao, X. Xu, *J. Electrochem. Soc.* **2015**, 163, A96; c) R. Xu, F. Han, X. Ji, X. Fan, J. Tu, C. Wang, *Nano Energy* **2018**, 53, 958; d) B. Zheng, J. Zhu, H. Wang, M. Feng, E. Umeshbabu, Y. Li, Q. H. Wu, Y. Yang, *ACS Appl. Mater. Interfaces* **2018**, 10, 25473; e) Y. Chen, W. Li, C. Sun, J. Jin, Q. Wang, X. Chen, W. Zha, Z. Wen, *Adv. Energy Mater.***2020**, 11, 2002545; f) H. Park, J. Kim, D. Lee, J. Park, S. Jo, J. Kim, T. Song, U. Paik, *Adv. Sci.* **2021**, 8, e2004204; g) Y. Li, W. Arnold, J. B. Jasinski, A. Thapa, G. Sumanasekera, M. Sunkara, B. Narayanan, T. Druffel, H. Wang, *Electrochim. Acta* **2020**, 363 137128; h) Y. Su, L. Ye, W. Fitzhugh, Y. Wang, E. Gil-González, I. Kim, X. Li, *Energy Environ. Sci.* **2020**, 13, 908; i) Z. Wang, Y. Jiang, J. Wu, Y. Jiang, W. Ma, Y. Shi, X. Liu, B. Zhao, Y. Xu, J. Zhang, *Nano Energy* **2021**, 84, 105906.

[18] a) F. Li, J. Liu, J. He, Y. Hou, H. Wang, D. Wu, J. Huang, J. Ma, *Angew. Chem. Int. Ed.* **2022**, 61, e202205091; b) J. Huang, J. Liu, J. He, M. Wu, S. Qi, H. Wang, F. Li, J. Ma, *Angew. Chem. Int. Ed.* **2021**, 60, 20717.

[19] a) H. Huo, J. Gao, N. Zhao, D. Zhang, N. G. Holmes, X. Li, Y. Sun, J. Fu, R. Li, X. Guo, X. Sun, *Nat. Commun.* **2021**, 12, 176; b) H. Huo, Y. Chen, R. Li, N. Zhao, J. Luo, J. G. Pereira da Silva, R. Mücke, P. Kaghazchi, X. Guo, X. Sun, *Energy Environ. Sci.* **2020**, 13, 127.

[20] a) T. Yersak, J. R. Salvador, R. D. Schmidt, M. Cai, *ACS Appl. Energy Mater.* **2019**, 2, 3523; b) G. Liu, W. Weng, Z. Zhang, L. Wu, J. Yang, X. Yao, *Nano Lett.* **2020**, 20, 6660; c) R. Song, R. Xu, Z. Wang, M. Yang, X. Yan, C. Yu,

10.1002/anie.202215680

L. Zhang, *J. Alloys Compd.* **2022**, 921, 166125; d) B. Zhao, Y. Shi, J. Wu, C. Xing, Y. Liu, W. Ma, X. Liu, Y. Jiang, J. Zhang, *Chem. Eng. J.* **2022**, 429, 132411; e) Y. Wang, D. Lu, J. Xiao, Y. He, G. J. Harvey, C. Wang, J.-G. Zhang, J. Liu, *Energy Storage Mater.* **2019**, 19, 80; f) R. Zhao, S. Kmiec, G. Hu, S. W. Martin, *ACS Appl. Mater. Interfaces* **2020**, 12, 2327; g) H. Wan, J. Zhang, J. Xia, X. Ji, X. He, S. Liu, C. Wang, *Adv. Funct. Mater.* **2022**, 32, 2110876.

[21] a) X. Chen, Z. Guan, F. Chu, Z. Xue, F. Wu, Y. Yu, *InfoMat* **2021,** 4, e12248; b) J. Liang, N. Chen, X. Li, X. Li, K. R. Adair, J. Li, C. Wang, C. Yu, M. Norouzi Banis, L. Zhang, S. Zhao, S. Lu, H. Huang, R. Li, Y. Huang, X. Sun, *Chem.Mater.* **2020**, 32, 2664.

[22] F. Zhao, S. H. Alahakoon, K. Adair, S. Zhang, W. Xia, W. Li, C. Yu, R. Feng, Y. Hu, J. Liang, X. Lin, Y. Zhao, X. Yang, T. K. Sham, H. Huang, L. Zhang, S. Zhao, S. Lu, Y. Huang, X. Sun, *Adv. Mater.* **2021**, 33, e2006577.

[23] J. Lee, T. Lee, K. Char, K. J. Kim, J. W. Choi, *Acc. Chem. Res.* **2021**, 54, 3390.

[24] R. Koerver, I. Aygün, T. Leichtweiß, C. Dietrich, W. Zhang, J. O. Binder, P. Hartmann, W. G. Zeier, J. Janek, *Chem. Mater.***2017**, 29, 5574.

[25] W. D. Jung, M. Jeon, S. S. Shin, J. S. Kim, H. G. Jung, B. K. Kim, J. H. Lee, Y. C. Chung, H. Kim, *ACS Omega* **2020**, 5, 26015.

[26] X. Yang, X. Gao, Q. Sun, S. P. Jand, Y. Yu, Y. Zhao, X. Li, K. Adair, L. Y. Kuo, J. Rohrer, J. Liang, X. Lin, M. N. Banis, Y. Hu, H. Zhang, X. Li, R. Li, H. Zhang, P. Kaghazchi, T. K. Sham, X. Sun, *Adv. Mater.* **2019**, 31, e1901220.

[27] F. Zhao, Y. Zhao, J. Wang, Q. Sun, K. Adair, S. Zhang, J. Luo, J. Li, W. Li, Y. Sun, X. Li, J. Liang, C. Wang, R. Li, H. Huang, L. Zhang, S. Zhao, S. Lu, X. Sun, *Energy Storage Mater.* **2020**, 33, 139.

[28] a) L. Wu, G. Liu, H. Wan, W. Weng, X. Yao, *J. Power Sources* **2021**, 491; b) J. Liang, X. Li, Y. Zhao, L. V. Goncharova, W. Li, K. R. Adair, M. N. Banis, Y. Hu, T. K. Sham, H. Huang, L. Zhang, S. Zhao, S. Lu, R. Li, X. Sun, *Adv. Energy Mater.***2019**, 9, 1902125; c) G. Yu, Y. Wang, K. Li, D. Chen, L. Qin, H. Xu, J. Chen, W. Zhang, P. Zhang, Z. Sun, *Sustain. Energy Fuels* **2021**, 5, 1211.

10.1002/anie.202215680

WILEY-VCH

RESEARCH ARTICLE

Entry for the Table of Contents

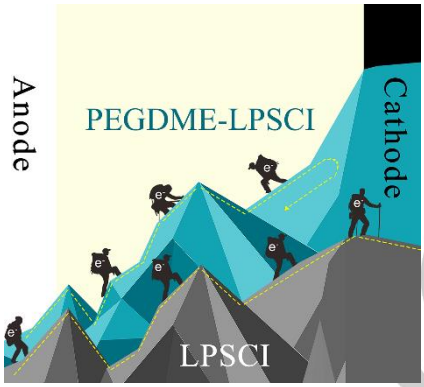

A grain boundary electronic insulation strategy is proposed to regulate the electronic conductivity of sulfide electrodes at the grain boundaries, which realizes dendrite- and self-discharge-free and humidity-stable all-solid-state lithium batteries.